Parameter-Topology Hybrid Optimization of Electric Motor with Multiple Permanent Magnets

Shogo Hayashi[a*], Hajime Igarashi[a]

[a]*Graduate School of Information Science and Technology, Hokkaido University, Sapporo 060-0814, Japan*

Abstract. A hybrid method that combines parameter optimization (PO) with topology optimization (TO) is proposed for the design of a permanent magnet (PM) motor. The PM shape, configuration, and flux barrier topology were simultaneously optimized using the proposed method. The conventional hybrid method that can deal with a single PM is effectively extended to deal with multiple PMs parameterized by several geometrical parameters. The use of this extension makes it possible to search for the optimal rotor structure of the multiple-PM motor, which is widely used in electric vehicles. The results obtained by the proposed method are superior to those obtained by conventional methods. The number of PMs can be increased to obtain a magnet configuration geometry suitable for the analytical model.

Keywords: Automatic mesh generation, parameter optimization (PO), permanent magnet (PM) motors, topology optimization (TO).

1 Introduction

Permanent magnet (PM) motors have high efficiency and high power density and are used in various electric devices, including motors for electric vehicles. A lot of research has been carried out to develop PM motors with superior characteristics [1-3]. Parameter optimization (PO) and topology optimization (TO) have been shown to be effective for improving the efficiency of PM motors [4-7]. In particular, the flux barrier and the shape and arrangement of the magnets in the rotor are crucial to improve the performance of the PM motor. In [4-6], the iron and air materials of the rotor are optimized by TO and motors with excellent characteristics is obtained. The boundary surfaces of materials obtained by TO are characterized by complexity. Because magnetic materials can be processed flexibly, the TO method is excellent for flux barrier optimization. On the other hand, the magnet shape of PM is generally limited to rectangular or fan shape due to the production method and cost. In addition to this, it is easy to define the design parameters of the magnet shape. Therefore the PO method is suitable for PM. An optimization method that hybridizes PO with TO methods was proposed in [8], which represented the PM shape and position by geometrical parameters for PO, whereas the flux barriers are represented by the shape function, which is a linear combination of the Gaussian basis functions for TO. The optimization variables for this TO are the weighting coefficients of the Gaussian functions. For the optimization, a stochastic algorithm, such as the genetic algorithm (GA) or covariance matrix adaptation evolution strategy (CMA-ES) [9], is adopted owing to the difficulty in evaluating the sensitivity of the objective function with respect to the geometrical parameters and weighting coefficients. Moreover, the stochastic algorithm can perform a global search, whereas gradient-based methods would lead to local minima. A large problem has remained in [8]; that is, a single PM is only considered and cannot move freely in the design region, although multiple PMs are widely employed for PM motors in electric vehicles.

In this study, the PO-TO hybrid method is extended to address multiple PMs. The proposed hybrid optimization method was applied to design the rotor shape of an internal PM (IPM) motor to maximize the average torque and minimize the torque ripple. The proposed method allows us to deal with multiple-PM motors that are integral for both electric vehicles and various electric systems. In the optimization process,
individuals with overlapping PMs were eliminated. The proposed method is compared with the conventional method and a sequential optimization method that sequentially performs PO and TO. Furthermore, on the basis of the proposed method, the performance of the optimal IPM motors that contain single, double and triple magnets are compered.

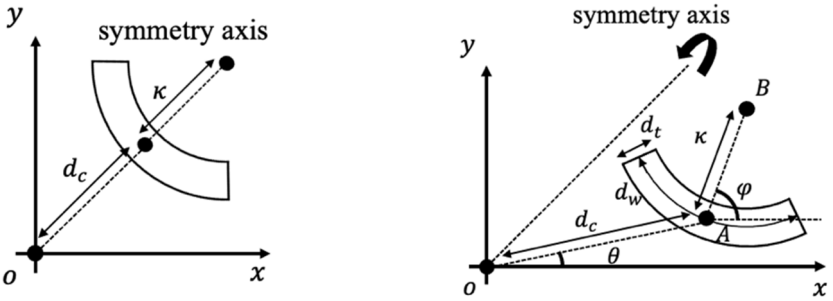

(a) Conventional parameter (b) Proposed representation

Fig. 1 Parameterization of PM

2 Proposed method

2.1 Parameter Optimization

In the design of IPM motors, there are constraints on the PM shape owing to limitations in volume, manufacturing process, and cost. The parameter representation of the PMs enables us to easily consider these constraints in the optimization process. Therefore, PO would be more beneficial for the optimization of PMs than TO. In [8], the curvature κ and distance d_c to the rotor axis were chosen as the optimization variables, as shown in Fig. 1(a). In this study, to consider more diverse PM configurations, the shape parameter $\boldsymbol{p}$ composed of $\{\theta, \varphi, d_t, d_w, d_c, \kappa\}$ defined in Fig. 1(b) is introduced, where A and B represent the rotor axis and center of curvature, respectively. In addition, it is assumed that multiple magnets can be used to consider various rotor structures. The magnets were replicated such that they were symmetrical about the symmetry axes.

2.2 Topology Optimization

The design of the rotor flux barrier is crucial for improving the torque performance and efficiency. In contrast to the optimization of PMs, it is difficult to preliminarily define design variables for flux barriers with flexible shapes. Therefore, topology optimization, which allows the generation and annihilation of holes and the free deformation of material boundaries, is effective for the optimization of flux barriers. Numerous methods are used for topology optimization, including sensitivity-based approaches, such as the level set method [10],[11] and density method [12], as well as stochastic approaches based on the normalized gaussian network (NGnet) applied to the ON/OFF method [13], [14]. In this study, the NGnet method was employed owing to its high searchability and lack of necessity for sensitivity computations. In this method, Gaussian basis functions are uniformly placed in the design region, and the material distribution is determined from the shape function defined by

$$\varphi(\boldsymbol{x}, \boldsymbol{w}) = \sum_{i=1}^{N} w_i b_i(\boldsymbol{x}) \tag{1},$$

where w_i indicates the weighting coefficient, $\boldsymbol{x}$ denotes the position vector, and N indicates the number of Gaussian basis functions. Moreover, $b_i(\boldsymbol{x})$ represents the normalized Gaussian basis function given by

$$b_i(\boldsymbol{x}) = \frac{G_i(\boldsymbol{x})}{\Sigma_{k=1}^{N} G_k(\boldsymbol{x})} \tag{2},$$

$$G_k(\boldsymbol{x}) = \frac{1}{2\pi\sigma^2} \exp\left[-\frac{\|\boldsymbol{x} - \boldsymbol{\mu}_k\|^2}{2\sigma^2}\right] \tag{3},$$

where $\boldsymbol{\mu}_k$ and σ^2 denote the center of the k-th Gaussian basis and variance, respectively. The material attribute v_e of a finite element e is determined by

$$A(\boldsymbol{x}, \boldsymbol{w}) \leftarrow \begin{cases} \text{air}, & \varphi < 0 \\ \text{iron}, & \varphi \geq 0 \end{cases} \tag{4}.$$

The material distribution depends on $\boldsymbol{w}$, which is determined to minimize the cost function. This means that topology optimization is reduced to parameter optimization with respect to $\boldsymbol{w}$.

2.3 *Improving Resolution of Shape Representation*

In a previous study on NGnet-based TO [14], a fixed finite element mesh was employed to determine the material of each element; this method, called the ON/OFF method, tends to produce a jagged shape, which causes difficulties in the manufacturing process. Although the resolution of the shape representation can be increased by making the fixed finite element mesh finer, this increases the computation time for finite element analysis (FEA). To avoid this problem, the FE meshes were adaptively generated as follows: We used open-source software (https://github.com/MmgTools/mmg) to generate a mesh that performs "implicit meshing" as proposed in [15]. As illustrated in Fig. 2, the values of the "level set" function are assigned to the vertices of a highly subdivided base mesh to generate a new mesh in which the material boundaries correspond to the 0-valued contours of the input level set function. The values of the shape function $\varphi(\boldsymbol{x}, \boldsymbol{w})$ given by (1) and the shape function $s(\boldsymbol{x}, \boldsymbol{p})$ which represent the shape of the magnet by a zero-valued contour, are input as level-set functions. The computational cost for mesh generation is much lower than that for FEA for static magnetic field analysis. The implicit mesh can be used to make the FE mesh coarser without losing accuracy, which leads to a reduction in the computation time for optimization.

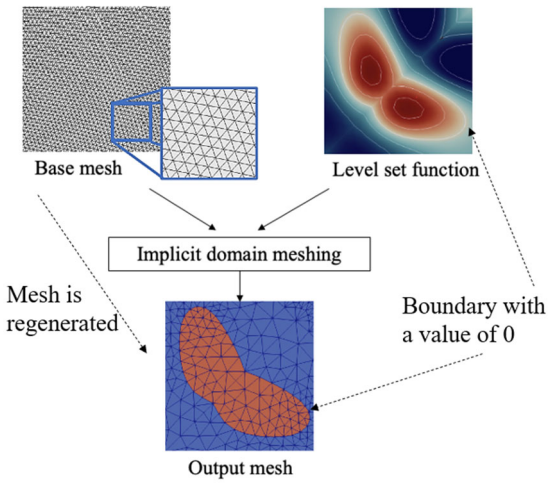

Fig.2 Flow of implicit-domain meshing

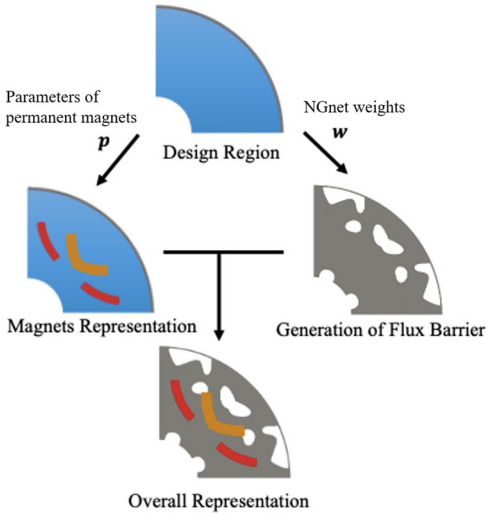

Fig.3 Representation of rotor shape

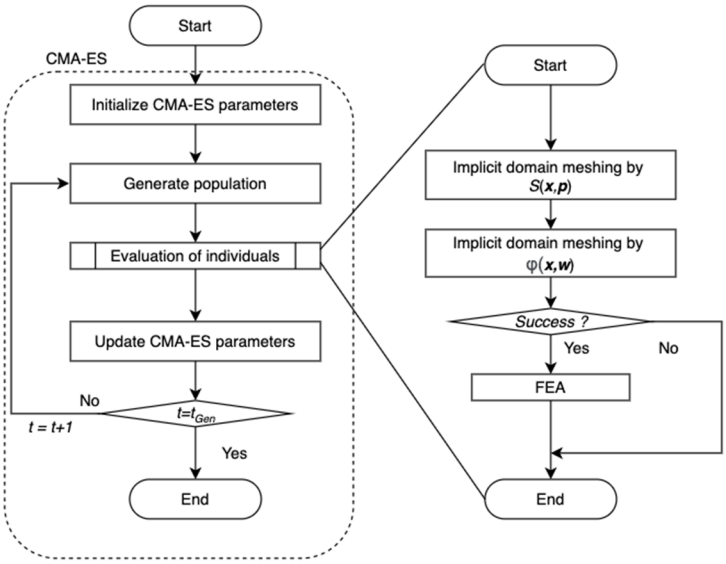

Fig. 4 Flow diagram of the optimization using CMA-ES

2.4 Optimization Procedure

As shown in Fig. 3, the rotor shape of the motor is determined by the PM parameters $\boldsymbol{p}$ and NGnet weights $\boldsymbol{w}$. The optimization problem is expressed as follows:

$$\text{minimize } f(\boldsymbol{p},\boldsymbol{w}), sub.\,to\ g_i(\boldsymbol{p},\boldsymbol{w}) \le 0,\ \ i = 0,1,2,\ldots \qquad (5).$$

where f and g_i denote objective function and constrains. This problem was solved using the CMA-ES [9]. The optimization flow diagram of the proposed method, where the stopping criterion is $t = t_{Gen}$ is illustrated in Fig. 4. For each individual that has unique values $\boldsymbol{p}$ and $\boldsymbol{w}$, mesh generation is performed by implicit mesh generation before FEA. Mesh generation may fail because of an unrealistic material distribution, which has, for example, extremely thin regions or multiple overlapping magnets. This also occurs for unacceptably flat finite elements. In such cases, FEA is not performed for that individual and a death penalty is added to the objective function.

3 Optimization Result

3.1 Effect of multiple PMs

We applied hybrid optimization to the model motor shown in Fig. 5. Considering the symmetry, the design region was set to half of the rotor region. Specifically, we assumed 60 Gaussian functions, $\sigma = 0.0015$, the centers of which were uniformly placed in the design region. In this problem, the position and shape of the two PMs and the flux barrier distribution were optimized. The optimization problem is defined as follows:

$$f(\boldsymbol{p},\boldsymbol{w}) = -\frac{T_{avg}}{T_{avg}^{ref}} + 0.2\frac{T_{rip}}{T_{rip}^{ref}} \to min. \qquad (6),$$

$$\text{sub. to } g_1(\boldsymbol{p},\boldsymbol{w}) = S_{mag} - S_{mag}^{ref} \le 0 \quad (7a), \qquad g_2(\boldsymbol{p},\boldsymbol{w}) = S_{demag} - 0.05\mathrm{S_{mag}} \le 0 \quad (7b),$$

$$g_3(\boldsymbol{p},\boldsymbol{w}) = n_{connect} - 1 \le 0 \quad (7c), \qquad g_4(\boldsymbol{p},\boldsymbol{w}) = -\min\left(\frac{S_{mag1}}{S_{mag2}}, \frac{S_{mag2}}{S_{mag1}}\right) + 0.3 \le 0 \quad (7d),$$

where T_{avg} and T_{rip} denote the average torque and torque ripple, respectively, S_{mag1} and S_{mag2} indicate the volumes of the two PMs, $S_{mag} = S_{mag1} + S_{mag2}$, where S_{demag} corresponds to the demagnetized PM area, $n_{connect}$ indicates the number of connected magnetic cores. The quantities indexed with *ref* denote those of the reference motor, as shown in Fig.6. Constraints g_1, g_2, g_3 and g_4 were introduced for the restriction that S_{mag} is smaller than S_{mag}^{ref}, the demagnetization area is less than 5%, the magnetic core is not separated into several cores, and tiny magnets that do not contribute to the torque performance are not present. For comparison, optimization using the conventional method with a single PM, shown in Fig.1, is performed. In addition, a sequential optimization was performed to verify the effectiveness of the hybrid PO-TO

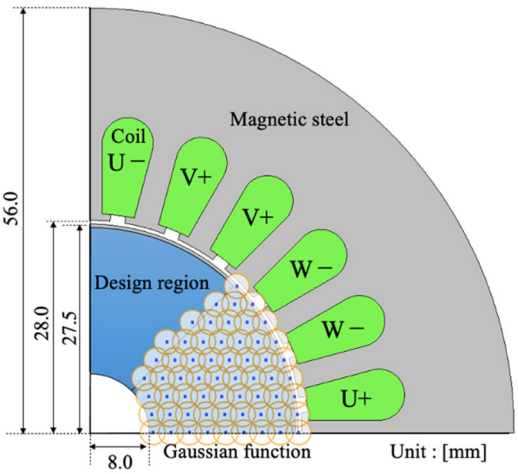

Fig. 5 Analysis motor. Circles represent the Gaussian functions.

Table 1 Parameters for FEA and CMA-ES

Number of genes	72, 62
Size of population	128
Number of generations	500
Range of θ [degree]	$0.0 \le \theta \le 45.0$
Range of φ [degree]	$-180 \le \varphi \le 180$
Range of d_t [mm]	$0.0 \le d_t \le 6.0$
Range of d_w [mm]	$0.0 \le d_w \le 50.0$
Range of d_c [mm]	$8.0 \le d_c \le 26.0$
Range of κ [mm^{-1}]	$0.0 < \kappa \le 100$
Current phase angle [degree]	40.0
Current amplitude [A]	10.0
Phases	3 phases
poles	4 poles
Coil Turns	35
Number of stator slot	24
Residual flux density	1.40
Electromagnetic Steel Sheets	50A400
Thickness [mm]	65

optimization, in which PO was performed for the PMs and TO was performed for the flax barriers. The settings for FEA and optimization are summarized in Table 1. In the proposed hybrid and sequential methods, the two magnets are represented by 12 parameters, such that the total design variables, including $\boldsymbol{w}$ are 72. In contrast, the design variable for the conventional method is 62. We used the hyper-parameters for CMA-ES, which are recommended in [9], except for the population size.

Table 2 summarizes the characteristics of the reference and optimized motors. Figs. 7 and 8 illustrate the rotor shapes and their torque waveforms optimized using the proposed, conventional, and sequential methods, respectively. Evidently, the motor obtained by the proposed method has the best properties: the highest value for T_{ave} and the lowest value for T_{rip}. In sequential optimization, the spacing between the PM and rotor surface is extremely narrow as a result of the PO. Therefore, flux barriers were not generated. The result suggests that the proposed hybrid method is superior to the sequential approach.

To consider the torques in detail, those are decomposed into magnet torque T_{mag} and reluctance torque T_{rel}. In this work, T_{mag} and T_{rel} were obtained from the magnet flux Φ_m and d- and q-axis self-inductance L_d, L_q, as follows:

$$T_{mag} = p\Phi_m i_q \quad (8a),$$

$$T_{rel} = p(L_d - L_q) i_d i_q \quad (8b),$$

where p indicates the number of pole pairs and i_d and i_q represent the d- and q-axis currents, respectively. The computed values of Φ_m, L_d, and L_q are summarized in Table 3, and the decomposed torques are illustrated in Fig. 9. The model obtained by the proposed method yields approximately 5% higher magnet torque and 20% higher reluctance torque than the IPM motor obtained by the conventional method. Under the conditions of this optimization, the IPM motor with double-U-shaped PMs effectively utilizes the reluctance torque by increasing the difference in the inductances between the d- and q-axis.

Fig. 6 Reference model

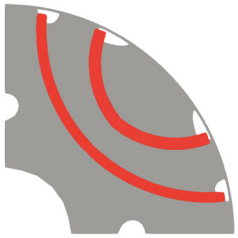

(a) Proposed method

(b) Conventional method

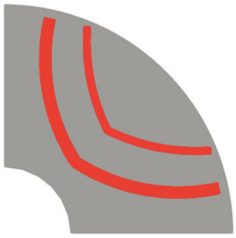

(c) sequential: PO → TO

Fig. 7 Optimization Results

Table 2 Characteristics of Reference and Optimized models

	f	T_{ave} [Nm]	T_{rip} [Nm]	S_{mag} [mm^2]
Ref. model	-0.80	6.61	3.97	78.4
Proposed method	-1.20	8.13	0.54	77.3
Conventional method	-1.10	7.64	1.19	78.4
Sequential method	-1.13	7.89	1.22	78.3

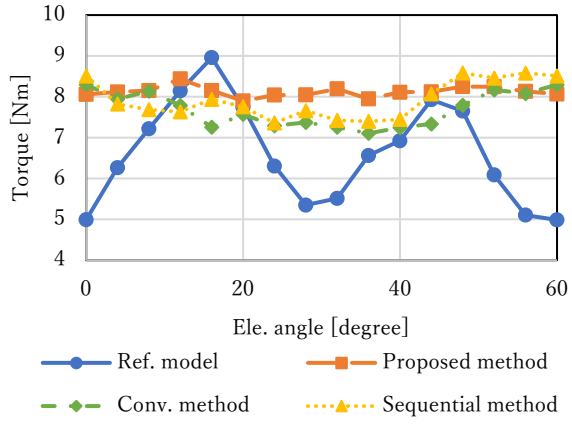

Fig. 8 Torque waveforms

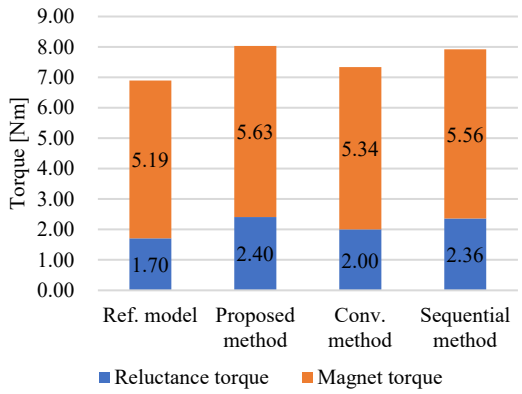

Fig. 9 Reluctance and magnet torque

Table 3 Characteristics of Reference and Optimized models

	Φ_a [Wb]	L_d [H]	L_q [H]
Ref. model	2.77×10^{-1}	6.66×10^{-3}	1.82×10^{-2}
Proposed method	3.00×10^{-1}	5.14×10^{-3}	2.14×10^{-2}
Conventional method	2.84×10^{-1}	5.14×10^{-3}	1.87×10^{-2}
Sequential method	2.97×10^{-1}	4.91×10^{-3}	2.09×10^{-2}

3.2 Effect of number of magnets

To compare the results of the proposed method with different numbers of magnets, optimization was performed by assuming single, double, and triple PMs. The design variables were 66 and 78 for single and triple magnets, respectively, and the other settings remained unchanged.
The characteristics of the optimization results are listed in Table 4. The resulting rotor shapes are illustrated in Fig. 10. We found that the performance of the single-PM motor was worse than that of the double- and triple-PM motors. Remarkably, triple-PM optimization results in double U-shaped PMs. The objective function is also almost the same as that of the double U-shaped PMs. The result suggests that a motor with double U-shaped PMs is the best under this optimization condition.

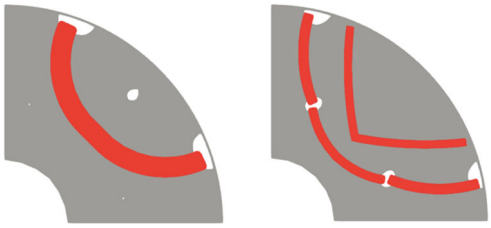

(a) Single magnet (b) Triple magnets
Fig. 10 Optimization results for different number of magnets

Table 4 Characteristics of Hybrid Optimized models for different number of magnets

	f	T_{ave} [Nm]	T_{rip} [Nm]	S_{mag} [mm^2]
Single magnet	-1.12	7.86	1.45	77.8
Triple magnets	-1.19	8.22	1.14	76.5

4 Conclusion

In this study, we successfully extended the conventional method by enriching the magnet parameters and increasing the possible number of PMs. The optimized results of the proposed method exhibited a better performance than those of the conventional method. Based on the results, it can be concluded that the IPM motor with double-U-shaped magnets provides the best torque performance among the classes that the proposed method can represent.

5 Acknowledgment

This work was supported in part by JSPS KAKENHI (Grant Number 21H01301).

References

[1] A. Balamurali, G. Feng, C. Lai, J. Tjong, and N. C. Kar, “Maximum effi- ciency control of PMSM drives considering system losses using gradient descent algorithm based on DC power measurement,” *IEEE Trans. Energy Convers*., vol. 33, no. 4, pp. 2240–2249, Dec. 2018.
[2] F. Niu et al., “A simple and practical duty cycle modulated direct torque control for permanent magnet synchronous motors,” *IEEE Trans. Power Electron*., vol. 34, no. 2, pp. 1572–1579, Feb. 2019.
[3] Pellegrino, G.; Cupertino, F., "FEA-based multi-objective optimization of IPM motor design including rotor losses," IEEE Energy Conversion Congress and Exposition (ECCE), 2010, vol., no., pp.3659-3666, 12-16 Sept. 2010
[4] H. Sasaki and H. Igarashi, Topology Optimization Accelerated by Deep Learning, *IEEE Transactions on Magnetics,* **55** (2019), 1–5.
[5] Y. Okamoto, Y. Tominaga, S. Wakao, and S. Sato, Topology optimization of rotor core combined with identification of current phase angle in IPM motor using multistep genetic algorithm, *IEEE Transactions on Magnetics,* **50** (2014), Art. no. 7017904.
[6] P. Gangl, S. Amstutz, and U. Langer, Topology optimization of electric motor using topological derivative for nonlinear magnetostatics, *IEEE Transactions on Magnetics*, **52** (2016), 1–4.
[7] J. S. Choi, K. Izui, S. Nishiwaki, A. Kawamoto, and T. Nomura, Topology optimization of the stator for minimizing cogging torque of ipm motors, *IEEE Transactions on Magnetics*, **47** (2011), 3024–3027.

[8] S. Hiruma, M. Ohtani, S. Soma, Y. Kubota, H. Igarashi, A Novel hybridization of parameter and topology optimizations: application to permanent magnet motor, *IEEE Transactions on Magnetics,* **57** (2021), 8204604.
[9] N. Hansen, The CMA evolution strategy: A tutorial, arXiv:1604.00772, 2016.
[10] J. Lee and S. Wang, Topological shape optimization of permanent magnet in voice coil motor using level set method, *IEEE Transactions on Magnetics*, **48** (2012), 931–934.
[11] Y. Yamashita and Y. Okamoto, Design optimization of synchronous reluctance motor for reducing iron loss and improving torque charac- teristics using topology optimization based on the level-set method, *IEEE Transactions on Magnetics*, **56** (2020), 1–4.
[12] F. Guo and I. P. Brown, Simultaneous magnetic and structural topology optimization of synchronous reluctance machine rotors, *IEEE Transactions on Magnetics*, **56** (2020), 1–12.
[13] T. Sato, K. Watanabe, and H. Igarashi, Multimaterial topology optimization of electric machines based on normalized Gaussian network, *IEEE Transactions on Magnetics*, **51** (2015), 1–4.
[14] H. Sasaki and H. Igarashi, Topology optimization using basis functions for improvement of rotating machine performances, *IEEE Transactions on Magnetics*, **54** (2018), 1–4.
[15] C. Dapogny, C. Dobrzynski, and P. Frey, Three-dimensional adaptive domain remeshing, implicit domain meshing, and applications to free and moving boundary problems, *Journal of Computational Physics*, **262** (2014), 358–378. doi: 10.1016/j.jcp.2014.01.005.